Microscopic analysis of extranuclear capture on the $^{16}O(p,\gamma)^{17}F$ reaction

D. Baye, P. Descouvemont, and M. Hesse
Physique Nucléaire Théorique et Physique Mathématique, C.P. 229, Université Libre de Bruxelles, B 1050 Brussels, Belgium
(Received 21 January 1998)

Starting from a fully microscopic calculation, the $^{16}O(p,\gamma)^{17}F$ radiative-capture reaction is discussed in detail. The generator-coordinate and microscopic R-matrix methods are applied to the determination of the bound states and phase shifts of the $^{16}O+p$ system, where ^{16}O is described by a closed p shell cluster. The astrophysical S factor is then calculated and compared with experiment. A study of its behavior at very low energies leads to general quantal formulas for the S factor and for its logarithmic derivative at zero energy, which are valid for all cases where capture dominantly occurs when both nuclei are far from each other. The larger capture to the $1/2^+$ excited state is then explained by its lower binding energy without need for a special halo effect. The logarithmic derivative at zero energy is shown to depend on a slowly varying function of the bound-state Sommerfeld parameter and its different values for capture to the $5/2^+$ and $1/2^+$ states are explained. The same expressions are applied to the $^7Be(p,\gamma)^8B$ reaction. [S0556-2813(98)00307-0]

PACS number(s): 25.40.Lw, 21.60.Gx, 24.10.Cn, 24.50.+g

I. INTRODUCTION

A precise knowledge of many radiative-capture reaction rates is essential for astrophysics [1]. Microscopic models of radiative-capture reactions [2–4] can provide a realistic description of astrophysical S factors down to very low energies (see Refs. [5–7] for reviews). They allow a parameter-free study of capture reactions. In microscopic models, antisymmetrization is exactly taken into account and the whole information is deduced from an effective nuclear force [8,9]. Strangely, these models have not been applied yet to a simple case, the $^{16}O(p,\gamma)^{17}F$ reaction, which leads to interesting physical considerations. The $^{16}O(p,\gamma)^{17}F$ reaction links different parts of the CNO cycle. It offers a clear example of applying the microscopic model. The ^{16}O nucleus is well described by a closed p shell configuration. The simpler potential or direct-capture model [10,11] also fairly well describes the energy dependence of the capture cross sections to the ^{17}F bound states. In fact, this reaction is one of the best examples of a capture mechanism usually called ''extranuclear capture'': At low energies, the capture process mostly occurs at distances much larger than the ^{16}O radius.

A detailed analysis of this effect is timely. During the completion of this work, the interest for this reaction was even increased by the issue of accurate new data which resolve the capture components to the ^{17}F ground state and to its single excited state down to about 200 keV [11]. These data emphasize the contrasted energy dependences of the S factors for capture to the $5/2^+$ ground state and $1/2^+$ excited state [10] which have not been explained yet with intuitive concepts. They also confirm the predicted fact [10] that the capture is stronger to the $1/2^+$ excited state of ^{17}F. Because of its low binding energy, this state has a larger spatial extension than the ground state. The authors of Ref. [11] attribute the larger S factor for capture towards this state and its low-energy rise to the existence of a proton halo in the $1/2^+$ wave function. Although no precise definition of a nuclear halo exists, this property is usually characterized by a radius which is significantly larger than the standard nuclear radius.

The aim of this paper is to present a fully microscopic study of the $^{16}O(p,\gamma)^{17}F$ reaction, performed with two effective nucleon-nucleon forces and to use it as a basis for discussing different physical issues. The questions we want to answer are the following. How do the microscopic results compare with experiment? What is their sensitivity to the choice of the nucleon-nucleon force? Can one understand and predict the very-low-energy behaviors of the S factors? Is the $1/2^+$ S-factor rise related to the existence of a proton halo in the excited state of ^{17}F?

At low energies, the capture process for some reactions like the present one or like $^7Be(p,\gamma)^8B$ is mostly extranuclear, i.e., takes place mostly when both nuclei are far away from each other (typically at several tens of fm). At such large distances, the Coulomb force largely dominates the nuclear interaction. Only two types of nuclear quantities may then influence the capture cross section, i.e., the asymptotic normalization constants of the bound states (or the related vertex constants) and the elastic scattering lengths. The influence of the former has been discussed in a number of papers (see Ref. [12] and references therein), but the role of the latter is usually disregarded. With its simple physical assumptions, the $^{16}O(p,\gamma)^{17}F$ reaction allows a detailed analysis of these effects. It is also a useful tool to validate indirect methods of determination of the astrophysical S factor by measuring asymptotic normalization constants, i.e., to test whether the knowledge of these constants is sufficient to provide an accurate S factor. The force sensitivity of these constants, which is an important problem for model calculations [12], can also be studied on this reaction.

In Sec. II, the microscopic model is described. In Sec. III, results about phase shifts, elastic cross sections and the radiative-capture astrophysical S factor are presented and compared with experiment. The low-energy behavior in the case of extranuclear capture is analyzed in a general context in Sec. IV. Physical aspects are discussed in Sec. V. Concluding remarks are presented in Sec. VI.

II. MICROSCOPIC MODEL

A. Cross sections

A radiative-capture reaction corresponds to an electromagnetic transition from an initial scattering state at the

center-of-mass energy E, towards a final bound state at energy $-E_B$. For an *electric* multipole transition of multipolarity λ, the capture cross section can be written as [3]

$$\sigma^{\mathrm{E}\lambda}_{l_iJ_i\to l_fJ_f}=\frac{8\pi}{\hbar}\,\frac{k_\gamma^{2\lambda+1}}{(2I_1+1)(2I_2+1)}\times\frac{\lambda+1}{\lambda(2\lambda+1)!!^2}\,\frac{2J_f+1}{2l_i+1}\times\sum_I\,|\langle\Psi^{J_f}_{l_f}||\mathcal{M}_{\mathrm{E}\lambda}||\Psi^{J_i}_{l_iI}(E)\rangle|^2, \tag{1}$$

where $k_\gamma=E_\gamma/\hbar c$ is the photon wave number and $E_\gamma=E+E_B$ is the photon energy. The colliding nuclei have spins I_1 and I_2 leading to a channel spin I. The orbital and total angular momenta are respectively l_f and J_f for the final wave function $\Psi^{J_f}_{l_f}$ and l_i and J_i for the initial wave function $\Psi^{J_i}_{l_iI}(E)$. The operator $\mathcal{M}_{\mathrm{E}\lambda\mu}$ appearing in the reduced matrix element is the electric multipole operator of rank λ. The initial and final wave functions appearing in Eq. (1), and in particular the normalization of $\Psi^{J_i}_{l_iI}$, will be defined in the next subsection.

By summing over the significant multipoles and initial states, one obtains the total capture cross section to a given final state. By eliminating the dominant part of Coulomb penetration effects, one defines the astrophysical S factor

$$S(E)=\sum_{l_fJ_f}S_{l_fJ_f}(E)=E\exp(2\pi\eta)\sum_{l_fJ_f}\sum_{l_iJ_i}\sum_\lambda\,\sigma^{\mathrm{E}\lambda}_{l_iJ_i\to l_fJ_f}, \tag{2}$$

where $\eta(E)$ is the Sommerfeld parameter.

B. Wave functions

The system is described by a 17-body microscopic Hamiltonian

$$H=\sum_{i=1}^{17}T_i+\sum_{i>j=1}^{17}V_{ij}, \tag{3}$$

where T_i is the kinetic energy of nucleon i and V_{ij} is the interaction (including Coulomb and spin-orbit) between nucleons i and j. Approximate solutions of Eq. (3) are required both at positive and negative energies.

The bound and scattering wave functions of the system will be described by resonating-group wave functions [8] as

$$\Psi^{JM}_l=\mathcal{A}\phi_O[\,\phi_p\otimes Y_l(\Omega_\rho)\,]^{JM}g_{lJ}(\rho), \tag{4}$$

where ϕ_O is the internal wave function chosen for ^{16}O $(I_1=0)$, ϕ_p is the spin-isospin state of the proton $(I_2=1/2)$, and $\boldsymbol{\rho}=(\rho,\Omega_\rho)$ is the quantal relative coordinate between the centers of mass of these clusters. The orbital momentum l coupled to the channel spin $I=1/2$ (which is omitted in this section) gives the total angular momentum J. The parity of this state is $(-)^l$.

The exact asymptotic form of a bound-state relative wave function in Eq. (4) is given by

$$g_{l_fJ_f}(\rho)=\rho^{-1}u_{l_fJ_f}(\rho)\underset{\rho\to\infty}{\to}C_{l_fJ_f}\rho^{-1}W_{-\eta_B,l_f+1/2}(2k_B\rho), \tag{5}$$

where the real numbers η_B and k_B are respectively the Sommerfeld parameter and the wave number of this bound state, and $W_{-\eta,l+1/2}$ is a Whittaker function [13]. The asymptotic normalization coefficient $C_{l_fJ_f}$ plays an important role at low energies. The asymptotic form of a scattering-state relative wave function can be written as

$$[4\pi(2l_i+1)]^{-1/2}g_{l_iJ_i}(\rho)=\rho^{-1}u_{l_iJ_i}(\rho)\underset{\rho\to\infty}{\to}v^{-1/2}(k\rho)^{-1}\times[\cos\delta_{l_iJ_i}F_{l_i}(k\rho)+\sin\delta_{l_iJ_i}G_{l_i}(k\rho)], \tag{6}$$

where F_l and G_l are the regular and irregular Coulomb functions [13]. In Eq. (6), v and k are respectively the relative velocity and wave number of the relative motion, and $\delta_{l_iJ_i}$ is the scattering phase shift. The unit-flux normalization is chosen consistently with Eq. (1).

A Slater determinant in the two-center harmonic-oscillator model is defined as

$$\Phi_K(\boldsymbol{R})=\mathcal{A}\Phi_O(-\tfrac{1}{17}\boldsymbol{R})\Phi_p(\tfrac{16}{17}\boldsymbol{R}), \tag{7}$$

where $\Phi_O(\boldsymbol{S})$ is a closed-shell s^4p^{12} Slater determinant and $\Phi_p(\boldsymbol{S})$ represents a $0s$ orbital (with spin and isospin), centered at $\boldsymbol{S}$. The subscript $K=\pm1/2$ corresponds to the proton spin projection. The internal wave functions ϕ_O and ϕ_p appearing in Eq. (4) differ from $\Phi_O(\boldsymbol{S})$ and $\Phi_p(\boldsymbol{S})$ by a Gaussian center-of-mass (c.m.) factor. The vector $\boldsymbol{R}$ joining the oscillator centers is the generator coordinate. A common oscillator parameter b is used on both centers. This Slater determinant is then projected on the orbital and total angular momenta as

$$\Phi^{JM}_l(R)=\frac{1}{4\pi}\sum_K\,(lIM-KK|JM)\times\int\,Y_l^{M-K}(\Omega_R)\Phi_K(\boldsymbol{R})d\Omega_R, \tag{8}$$

where $\boldsymbol{R}=(R,\Omega_R)$.

Initial and final wave functions are expanded as

$$\Psi^{JM}_l=\sum_{n=1}^{N}f^J_{ln}\Phi^{JM}_l(R_n), \tag{9}$$

where N is the number of selected generator coordinates. The generator-coordinate values are usually chosen equidistant. Expression (9) is equivalent to Eq. (4) except for a Gaussian c.m. factor (not written here for simplicity) whose effect can be eliminated exactly and easily [3,9]. The relative function g_{lJ} depends on the coefficients f^J_{ln} which must be derived from the Hamiltonian H.

The expressions (9) and (8) provide fair simple approximations of the ^{17}F bound states at small separation distances between the ^{16}O and p clusters. However the asymptotic properties of these bound states display a Gaussian decrease which is not realistic at large distances since it disagrees with Eq. (5). A similar problem occurs for scattering states whose

oscillating asymptotic behavior (6) cannot be simulated by a finite number of square-integrable functions. Expression (9) will therefore only be used in a limited range of ρ values and the correct asymptotic forms (5) and (6) will be obtained with the help of the microscopic R-matrix method.

C. Microscopic R-matrix method

In the R-matrix formalism [14,3,9], the configuration space is divided into two regions, separated at a distance a, the ''channel radius.'' In the internal region ($\rho \leqslant a$), the internal wave function $\Psi^{JM}_{l,\mathrm{int}}$ is described by approximation (9) in the microscopic cluster model, with full account of antisymmetrization. In the external region ($\rho > a$), the external wave function $\Psi^{JM}_{l,\mathrm{ext}}$ involves a relative wave function g_{lJ} approximated by its exact asymptotic form (5) or (6); the antisymmetrization and the nuclear interaction between nucleons belonging to remote nuclei are neglected.

The physics of the problem is deduced from the Bloch-Schrödinger equation [14,3,9]

$$(H+\mathcal{L}-E)\Psi^{JM}_{l,\mathrm{int}} = \mathcal{L}\Psi^{JM}_{l,\mathrm{ext}}, \tag{10}$$

in which the left-hand side (LHS) involves the wave function $\Psi^{JM}_{l,\mathrm{int}}$ in the internal region and the RHS involves the asymptotic form $\Psi^{JM}_{l,\mathrm{ext}}$ of the wave function. The Bloch operator $\mathcal{L}$ is a surface operator [proportional to $\delta(\rho-a)$] which imposes the continuity of the logarithmic derivatives of the two components of the wave function [15]. The internal and external wave functions are in addition related by the continuity condition

$$\Psi^{JM}_{l,\mathrm{int}}(a) = \Psi^{JM}_{l,\mathrm{ext}}(a), \tag{11}$$

in which the RHS is known, except for a normalization factor at negative energies or for a dependence on the scattering matrix at positive energies.

The main advantage of the microscopic R-matrix method is that it provides theoretical R-matrices which, for a single channel, read as

$$R_{lJ}(E) = \sum_{\nu=1}^{N} \frac{\gamma^2_{lJ\nu}}{E_{lJ\nu}-E}, \tag{12}$$

where $\gamma_{lJ\nu}$ is the reduced width amplitude associated with pole $E_{lJ\nu}$. Contrary to the phenomenological R-matrix employed in fits of experimental data, this theoretical R-matrix is completely determined by the Schrödinger equation with Hamiltonian (3) and does not rely on experiment. It possesses N poles obtained from approximately solving Eq. (10). The phase shift deduced from $R_{lJ}(E)$ must be (almost) independent of the value of the channel radius a.

The Bloch-Schrödinger equation provides bound-state and scattering wave functions made of two pieces $\Psi^{JM}_{l,\mathrm{int}}$ and $\Psi^{JM}_{l,\mathrm{ext}}$ which can now be used to calculate the radiative-capture matrix element appearing in Eq. (1).

D. Matrix elements

The Bloch-Schrödinger equation (10) is solved by projection on the basis states (8). The cross sections are then calculated with Eq. (1). Because of the split structure of the wave function, the matrix elements must be calculated in several parts.

The calculation of the different matrix elements of the overlap, kinetic, central and spin-orbit nuclear interactions, and Coulomb interaction follows a standard procedure [3,9]. Here we shall just briefly explain the calculation of the $E1$ transition matrix element. The first and most difficult part is performed over the full configuration space with basis functions (8). The microscopic $E1$ operator reads

$$\mathcal{M}_{\mathrm{E1}\mu} = e\sum_{i=1}^{17} (\tfrac{1}{2}-t_{i3})(r_{i\mu}-R_{\mathrm{cm}\mu}), \tag{13}$$

where t_{i3} is the third component of the isospin operator of nucleon i, $r_{i\mu}$ ($\mu = x$, y, or z) is a component of its coordinate $\boldsymbol{r}_i$, and $R_{\mathrm{c.m.}\mu}$ is a component of the c.m. coordinate. With separate calculations for the one-body and c.m. parts of this matrix element, one obtains

$$\langle \Phi_K(\boldsymbol{R})|\mathcal{M}_{\mathrm{E1}\mu}|\Phi_{K'}(\boldsymbol{R}')\rangle = -\tfrac{4}{17}e(R_\mu+R'_\mu)\langle \Phi_K(\boldsymbol{R})|\Phi_K(\boldsymbol{R}')\rangle\delta_{KK'}, \tag{14}$$

where the overlap is given by

$$\langle \Phi_K(\boldsymbol{R})|\Phi_K(\boldsymbol{R}')\rangle = \exp[-4(\boldsymbol{R}-\boldsymbol{R}')^2/17b^2][1-\exp(-\boldsymbol{R}\cdot\boldsymbol{R}'/2b^2) \times (1+\boldsymbol{R}\cdot\boldsymbol{R}'/2b^2)]. \tag{15}$$

The reduced $E1$ matrix element between projected basis states is then given for $l_f = l_i - 1$ by

$$\langle \Phi^{J_f}_{l_f}(R)||\mathcal{M}_{\mathrm{E1}}||\Phi^{J_i}_{l_i}(R')\rangle = 2\pi^2(-1)^{l_f+J_i+I}\left[\frac{2J_i+1}{l_i(2l_i-1)(2l_i+1)}\right]^{1/2}\begin{Bmatrix} J_i & l_i & 1/2 \\ l_f & J_f & 1 \end{Bmatrix}\left[l_i\int_{-1}^{1} P_{l_i}(\cos\theta) \times\langle \Phi_K(\boldsymbol{R})|\mathcal{M}_{\mathrm{E1}z}|\Phi_K(\boldsymbol{R}')\rangle d\cos\theta + \int_{-1}^{1} P^1_{l_i}(\cos\theta)\langle \Phi_K(\boldsymbol{R})|\mathcal{M}_{\mathrm{E1}x}|\Phi_K(\boldsymbol{R}')\rangle d\cos\theta\right], \tag{16}$$

TABLE I. Potential parameters m or u and S_0 (in MeV fm^5) and asymptotic normalization constants $C_{l_f J_f}$ (in fm$^{-1/2}$).

N	Potential	m or u	S_0	$C_{d5/2}$	$C_{s1/2}$
8	V2	0.59359	23.39	1.0935	91.15
10	V2	0.59370	23.45	1.0934	91.14
8	MN	0.91790	33.77	0.9734	86.20
10	MN	0.91728	33.92	0.9731	86.42

where θ is the angle between $\boldsymbol{R}$ and $\boldsymbol{R}'$, P_l is a Legendre polynomial, and P_l^1 is an associated Legendre function. The integration over θ in Eq. (16) is performed numerically with a Gauss quadrature.

The basis states (8), and therefore the wave function (9), are only valid in the internal region. Let us briefly sketch the rest of the calculation (see Ref. [3] for details). Subtracting a correction over the external region involving the same basis states provides the $E1$ matrix elements over the internal region. This correction is simple since antisymmetrization can be neglected. It involves a one-dimensional integral which is performed numerically. Then adding the exact asymptotic form of the $E1$ matrix elements leads to the values to be used in Eq. (1) from which the S factor is deduced with Eq. (2). This one-dimensional integral involves the Whittaker and Coulomb functions appearing in the asymptotic forms (5) and (6). Special care must be taken in the numerical integration of this part of the correction since the low binding energies of the final states lead to a very slow decrease of the integrand.

III. RESULTS

The ^{16}O nucleus is well described by a closed-shell s^4p^{12} harmonic-oscillator configuration with the oscillator parameter $b=1.76$ fm which reproduces the ^{16}O radius $\langle r^2\rangle^{1/2}=2.58$ fm, corresponding to a charge radius of 2.71 fm. Two sets of generator coordinates have been selected in order to test the sensitivity to this choice: $N=8$ values from 1.7 to 10.1 fm with a step of 1.2 fm and $N=10$ values from 0.9 to 9.9 fm with a step of 1.0 fm. The channel radius is taken in both cases as 8.9 fm, but we have checked that the results are stable enough with respect to variations of a. The interest of using the R-matrix method is striking here: our basis only extends up to about 10 fm while integrals in matrix elements reach 300 fm. The basis states must only cover the region where the nuclear interaction and antisymmetrization between the incoming proton and ^{16}O are not negligible.

Two effective nucleon-nucleon interactions are employed: V2 (Ref. [16]) and Minnesota (hereafter referred to as MN, Ref. [17]). Their exchange parameter m or u and their spin-orbit amplitude S_0 [18] are slightly adjusted to reproduce the ^{17}F bound spectrum, i.e., $5/2^+$ and $1/2^+$ states respectively located 0.6005 and 0.1052 MeV below threshold. The conditions of the calculations are given in Table I. With those parameters, the energies are reproduced within 0.1 keV. Since comparisons require fitting the energies, the parameters are slighly different for the two sets of generator coordinates. The asymptotic normalization constants $C_{l_f J_f}$ defined in Eq. (5) are also displayed in Table I. Even for the weakly bound $1/2^+$ state, they are not much sensitive to the choice of basis states. As discussed in Sec. V, they are sensitive to the interaction choice.

TABLE II. Root-mean-square radii (in fm), quadrupole moment (in e fm^2), and reduced $E2$ transition probability (in W.u.) in the ^{17}F spectrum.

	V2	MN	Expt.
$\langle r^2\rangle^{1/2}(5/2^+)$	2.67	2.65	
$\langle r^2\rangle^{1/2}(1/2^+)$	2.79	2.77	
$Q(5/2^+)$	-8.0	-7.3	$\pm(10\pm2)$
$B(E2,1/2^+\rightarrow5/2^+)$	23.6	19.1	25.0 ± 0.5

Different spectroscopic quantities are gathered in Table II. With $N=8$ basis states, the table would be identical except for both $B(E2)$ which would be smaller by 1.5%. The results obtained with MN are slightly smaller than those obtained with V2. The agreement with the experimental quadrupole moment [19] is reasonable if we assume that it is negative, but the reduced $E2$ transition probability is somewhat too small. The rms radius of the excited state is larger by about 0.12 fm than the ground-state one, i.e., by 4%. The larger difference presented in Ref. [11] corresponds to the rms radius $\langle\rho^2\rangle^{1/2}$ of the relative motion of the loosely bound proton.

Elastic phase shifts obtained with both interactions and $N=10$ are displayed in Fig. 1. The results with $N=8$ would not be distinguishable except in the $3/2^+$ resonance whose location differs by less than 0.1 MeV. According to the generalized Levinson theorem [20], the phase shifts at zero energy are defined as $\pi(m_{lJ}+n_{lJ})$ where m_{lJ} is the number of forbidden states (1 in the s and p waves and 0 beyond) and n_{lJ} is the number of bound states in the corresponding partial wave. The positive-parity phase shifts (upper part) are in good agreement with those deduced from experiment [21], except in the vicinity of the $3/2^+$ resonance whose amplitude is not well reproduced by the MN force (full lines) and whose location is not well reproduced by the V2 force (dotted lines). A narrow $1/2^-$ resonance and a broad $3/2^-$ resonance which have a more complicated structure than $^{16}\mathrm{O}_{\mathrm{g.s.}}+p$ do not appear on the negative parity phase shifts (lower part). The present phase shifts are comparable to those obtained in Ref. [22].

Elastic excitation functions at a laboratory angle of 166° obtained with both interactions are presented in Fig. 2 where they are compared with data of Ref. [23]. The MN cross sections agree on the average with experiment. The complicated structure due to the overlapping $3/2^+$ and $3/2^-$ resonances can not be reproduced by the present model. The V2 cross sections are rather poor mostly because the $3/2^+$ resonance is not located at a correct energy.

Finally, let us come to radiative capture. Capture occurs mostly through an $E1$ transition from the initial p wave to the final $d5/2^+$ and $s1/2^+$ bound states. The small f components in $E1$ capture are included in the calculation and we have checked that $E2$ capture leads to negligible contributions. Then, without any fit or effective charge, the astrophysical S factor is obtained as shown in Fig. 3. Strikingly, the capture towards the $1/2^+$ excited state is larger than the capture towards the $5/2^+$ ground state. This will be discussed

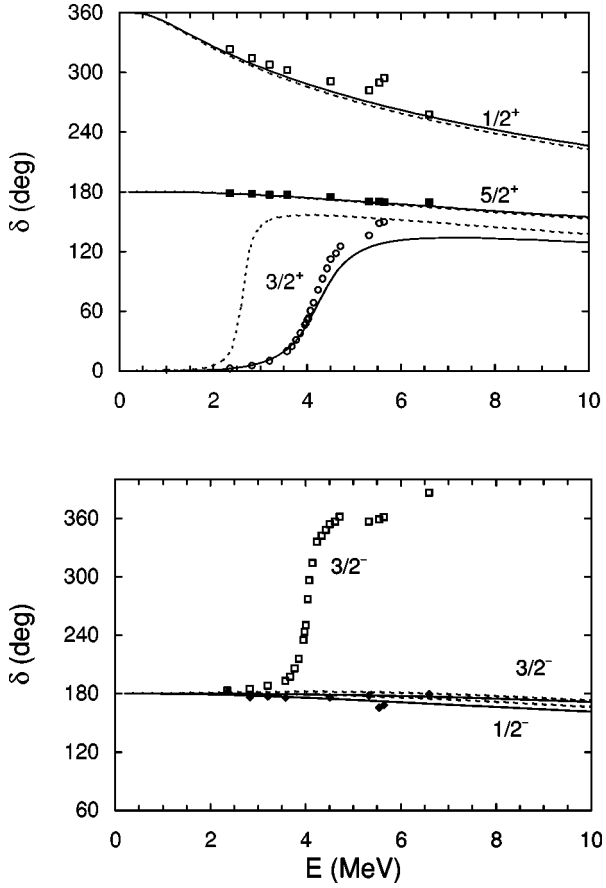

FIG. 1. Phase shifts δ_{lJ} for the $^{16}O+p$ elastic scattering as a function of the c.m. energy E for the $1/2^+$, $3/2^+$, and $5/2^+$ partial waves (upper part), and for the $1/2^-$ and $3/2^-$ partial waves (lower part) calculated with the MN (full lines) and V2 (dotted lines) forces. Experimental phase shifts are from Ref. [21].

in detail in Sec. V on the basis of a general analysis of extranuclear capture performed in the next section.

The shapes of the theoretical curves are in good agreement with recent absolute [11] and relative [10] data. For ground-state capture, the absolute normalization seems to be too small with MN and too large with V2. For the dominant capture to the $1/2^+$ state, the normalization is better with the

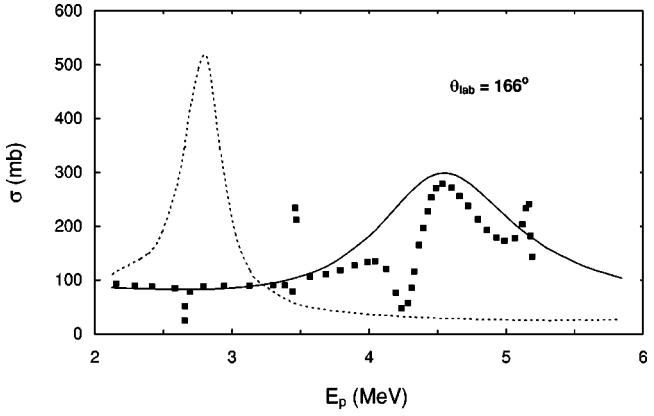

FIG. 2. Excitation functions for the $^{16}O+p$ elastic scattering as a function of the proton energy E_p at a laboratory angle of 166°, calculated with the MN (full lines) and V2 (dotted lines) forces. Experimental cross sections are from Ref. [23].

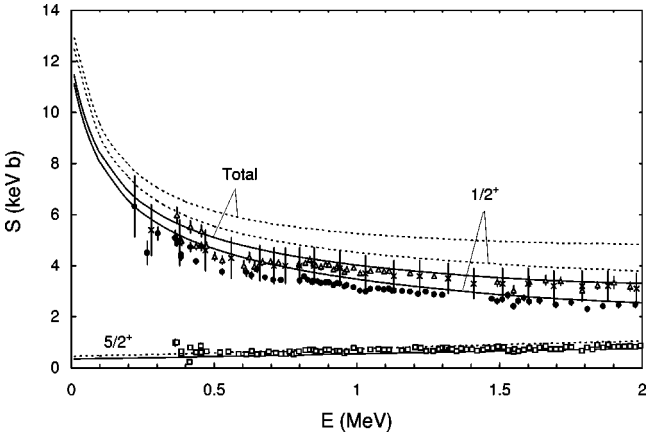

FIG. 3. Astrophysical S factor for the $^{16}O(p,\gamma)^{17}F$ reaction as a function of the c.m. energy E, calculated with the MN (full lines) and V2 (dotted lines) forces. From bottom to top: $5/2^+$ ground-state, $1/2^+$ excited-state and total captures. Experimental S factors from Ref. [10] (total: crosses) and Ref. [11] ($5/2^+$: squares, $1/2^+$: circles, total: triangles).

MN interaction (full line) than with V2 (dotted line) but both calculations overestimate the data. Of course, this overestimation affects the total S factors. This effect and $S(0)$ values will also be discussed in Sec. V.

IV. ANALYTICAL STUDY OF EXTRANUCLEAR CAPTURE AT LOW ENERGIES

The rise of the S factor at low energies is confirmed by experiment. Its origin can not easily be explained intuitively but arises from asymptotic properties of the Coulomb wave functions. Let us study this effect in the general case where external capture dominates, for two nuclei with mass numbers A_1 and A_2 $(A=A_1+A_2)$, charges Z_1e and Z_2e, and spins I_1 and I_2.

When the capture is essentially extranuclear, antisymmetrization and other short-distance effects can be neglected and the S factor in Eq. (2) can be approximated as

$$S_{l_fJ_f}(E)=\alpha c N_{E\lambda} k_\gamma^{2\lambda+1}\left(\int_{r_0}^{\infty} u_{l_fJ_f}\rho^\lambda \tilde{u}_{l_i}(E)d\rho\right)^2, \quad (17)$$

where α is the fine structure constant, r_0 is a cutoff radius, and

$$N_{E\lambda}=8\pi\left[Z_1\left(\frac{A_2}{A}\right)^\lambda+Z_2\left(-\frac{A_1}{A}\right)^\lambda\right]^2 \times\frac{(\lambda+1)(2\lambda+1)}{\lambda(2\lambda+1)!!^2}\frac{(2J_f+1)(2l_i+1)}{(2I_1+1)(2I_2+1)}\begin{pmatrix} l_f & \lambda & l_i \\ 0 & 0 & 0\end{pmatrix}^2 \quad (18)$$

is a normalization factor. The asymptotic form of $u_{l_fJ_f}$ also depends on the channel spin I. In order to keep the notations simple, we do not write this quantum number explicitly. A sum over I is understood in Eq. (17). At very low energies, the renormalized function

$$\tilde{u}_l(E)=E^{1/2}\exp(\pi\eta)u_l(E) \quad (19)$$

weakly depends on energy. Since the phase shifts are very small at these energies and since large distances ρ are considered, the shape of $\tilde{u}_l$ mostly depends on the orbital momentum l. Its dependence on other quantum numbers can approximately be taken into account through some average of the different phase shifts corresponding to l [see Eq. (28) below]. The overlap between the exponentially decreasing wave function $u_{l_f J_f}$ of the final bound state and the exponentially increasing wave function $\tilde{u}_{l_i}$ of the low-energy scattering state peaks at large distances. For example, in the $^{16}\mathrm{O}(p,\gamma)^{17}\mathrm{F}$ case, the maximum of the integrand in Eq. (17) occurs near 18 fm for the ground state and near 67 fm for the $1/2^+$ state.

Let us expand the S factor near zero energy as

$$S(E)=S(0)(1+s_1E+\cdots), \tag{20}$$

where a precise value of the logarithmic derivative at the origin

$$s_1=\frac{1}{S(0)}\left(\frac{dS}{dE}\right)_0 \tag{21}$$

is important for a correct evaluation of reaction rates.

First, let us calculate $S(0)$. To this end, we introduce the ''nuclear Bohr radius''

$$a_N=\hbar^2/\mu Z_1 Z_2 e^2 \tag{22}$$

and the ''nuclear Rydberg energy'' or ''Gamow energy''

$$E_N=\hbar^2/2\mu a_N^2. \tag{23}$$

Not surprisingly, when the Coulomb interaction dominates, nuclear analogs of the atomic units appear. From Ref. [24], we establish a connection with the modified Bessel functions,

$$\lim_{E\to 0} k^{-1/2}\exp(\pi\eta)F_l(k\rho)=\pi^{1/2}\rho^{1/2}I_{2l+1}(x) \tag{24}$$

and

$$\lim_{E\to 0} k^{-1/2}\exp(-\pi\eta)G_l(k\rho)=2\pi^{-1/2}\rho^{1/2}K_{2l+1}(x) \tag{25}$$

with

$$x=2(2\eta k\rho)^{1/2}=2(2\rho/a_N)^{1/2}. \tag{26}$$

In Eq. (25), we follow the sign convention of Ref. [13], where the K_n are positive functions, rather than the convention of Ref. [24]. From these relations, the limit of $\tilde{u}_{l_i}(E)$ can be approximated to first order with respect to scattering lengths as

$$\tilde{u}_{l_i}(0)=(\pi\hbar/2)^{1/2}\rho^{1/2}[I_{2l_i+1}(x)-4(a_{l_i}/a_N)K_{2l_i+1}(x)]. \tag{27}$$

In Eq. (27), we make use of the average scattering length defined as

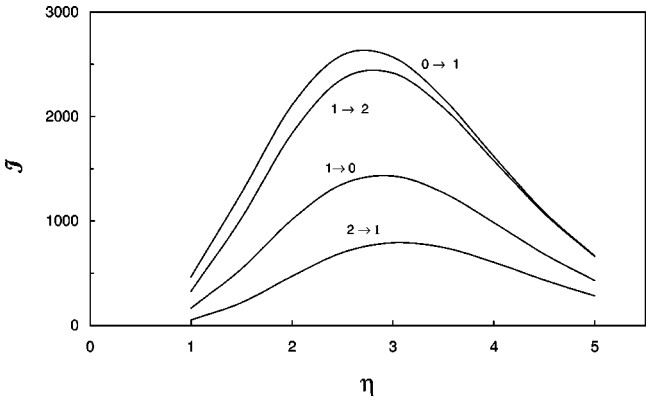

FIG. 4. Functions $\mathcal{I}_{1l_il_f}$ [Eq. (31) with $x_0=2$] as a function of η, for the $E1$ transitions $l_i=0\to l_f=1$, $l_i=1\to l_f=0$, $l_i=1\to l_f=2$, and $l_i=2\to l_f=1$.

$$a_{l_i}=-\frac{a_N}{2\pi}(2l_f+1)\sum_{J_i}(2J_i+1)\begin{Bmatrix} J_i & l_i & I \\ l_f & J_f & \lambda \end{Bmatrix}^2 \times \lim_{E\to 0}\exp(2\pi\eta)\,\delta_{l_iIJ_i}(E). \tag{28}$$

This expression may depend on λ, l_f, I, and J_f. Introducing the resulting expression (27) in Eq. (17) provides

$$S(0)=\tfrac{1}{2}\pi\alpha\hbar c N_{\mathrm{E}\lambda}(E_B/\hbar c)^{2\lambda+1} \times\left\{\int_{r_0}^{\infty} u_{l_fJ_f}\rho^{\lambda+1/2}[I_{2l_i+1}(2\sqrt{2\rho/a_N}) -4(a_{l_i}/a_N)K_{2l_i+1}(2\sqrt{2\rho/a_N})]d\rho\right\}^2. \tag{29}$$

The same principle was applied in Ref. [25] for calculating $S(0)$ for the reaction $^3\mathrm{He}(\alpha,\gamma)^7\mathrm{Be}$, but with numerical wave functions for $\tilde{u}_{l_i}(0)$ and $u_{l_fJ_f}$.

As confirmed in the next section, the second term in the brackets of Eq. (29) is often very small when external capture dominates, because $I_n(x)$ and $K_n(x)$ respectively behave as increasing and decreasing exponentials for large values of their argument x. Neglecting this term and replacing $u_{l_fJ_f}$ by its asymptotic form [see Eq. (5)] yields the expression

$$S(0)=\frac{\pi}{32}\alpha\hbar c a_N^2 N_{\mathrm{E}\lambda}(a_N E_B/8\hbar c)^{2\lambda+1}[C_{l_fJ_f}\mathcal{I}_{\lambda l_i l_f}(\eta_B)]^2. \tag{30}$$

The dimensionless functions

$$\mathcal{I}_{\lambda l_i l_f}(\eta)=\int_{x_0}^{\infty} W_{-\eta,l_f+1/2}(x^2/4\eta)x^{2\lambda+2}I_{2l_i+1}(x)dx \tag{31}$$

with $x_0=\sqrt{8r_0/a_N}$ mostly depend on η. For $E1$ transitions, they are depicted in Fig. 4 for the important cases $l_i=0\to l_f=1$, $l_i=1\to l_f=0$, $l_i=1\to l_f=2$, and $l_i=2\to l_f=1$. Typical values of x_0 are 1 for light systems and 2 to 3 for the present case. Here we choose $x_0=2$. Consistently with the extranuclear capture assumption, we assume $\eta>1$. The four

functions display the same shape, with a maximum around $\eta=3$. They have the same order of magnitude but $\mathcal{I}_{110}$ and $\mathcal{I}_{121}$ are smaller than the other two. The binding-energy dependence of $S(0)$ will be less sensitive to $\mathcal{I}_{\lambda l_i l_f}$ than to the power factor $E_B^{2\lambda+1}$.

The energy derivative of the S factor at zero energy can be treated in a similar way. A direct calculation of s_1 based on other expansions of the Coulomb functions was performed in Ref. [26]. In Eq. (17), only k_γ and $\tilde{u}_{l_i}$ depend on energy. Hence, s_1 can be expressed as [7]

$$s_1=\frac{2\lambda+1}{E_B}+2\frac{\int_{r_0}^{\infty}u_{l_f J_f}\rho^{\lambda}\left(\frac{d}{dE}\tilde{u}_{l_i}\right)_0 d\rho}{\int_{r_0}^{\infty}u_{l_f J_f}\rho^{\lambda}\tilde{u}_{l_i}(0)d\rho}. \tag{32}$$

This expression only depends on the extranuclear approximation and on the cutoff radius r_0. It is an exact quantum mechanical result within this assumption when scattering lengths are negligible. It still depends on nuclear effects through the binding energy E_B and, possibly, through the average scattering length in $\tilde{u}_{l_i}$.

Since $\eta^{-2}=E/E_N$, the limit of the energy derivative

$$\lim_{E\to 0}\frac{d}{dE}\left[k^{-1/2}\exp(\pi\eta)F_l(k\rho)\Big/\prod_{n=1}^{l}\left(1+\frac{n^2}{\eta^2}\right)\right]$$
$$=-\frac{\pi^{1/2}}{12E_N}\rho^{1/2}\left(\frac{x}{2}\right)^2\left[\frac{x}{2}I_{2l+2}(x)+lI_{2l+3}(x)\right] \tag{33}$$

can be deduced from expansion (6.12) in Ref. [24]. It provides, when the contribution of the scattering length is negligible,

$$s_1=E_B^{-1}[2\lambda+1-\mathcal{R}_{\lambda l_i l_f}(\eta_B)] \tag{34}$$

with the dimensionless functions

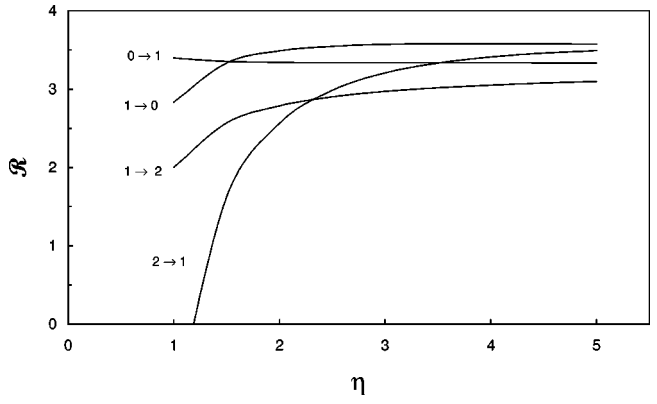

FIG. 5. Functions $\mathcal{R}_{1l_i l_f}$ [Eq. (35) with $x_0=2$] as a function of η, for the $E1$ transitions $l_i=0\to l_f=1$, $l_i=1\to l_f=0$, $l_i=1\to l_f=2$, and $l_i=2\to l_f=1$.

$$\mathcal{R}_{\lambda l_i l_f}(\eta)=\frac{1}{6\eta^2}\left[\frac{\mathcal{I}_{\lambda+3/2,l_i+1/2,l_f}(\eta)+2l_i\mathcal{I}_{\lambda+1,l_i+1,l_f}(\eta)}{8\mathcal{I}_{\lambda l_i l_f}(\eta)}\right.$$
$$\left.-l_i(l_i+1)(2l_i+1)\right]. \tag{35}$$

For $E1$ transitions, these functions are depicted in Fig. 5 for $l_i=0\to l_f=1$, $l_i=1\to l_f=0$, $l_i=1\to l_f=2$, and $l_i=2\to l_f=1$ $(x_0=2)$. The first three functions do not vary much with η but $\mathcal{R}_{121}$ displays a stronger dependence. Their variations have important consequences on the low-energy behavior of the S factor. Their values have to be compared with the critical value $2\lambda+1=3$ appearing in Eq. (34). The function $\mathcal{R}_{101}$ is always larger than 3 so that s_1 will be negative for any η_B like in the $^7\mathrm{Be}(p,\gamma)^8\mathrm{B}$ reaction. The function $\mathcal{R}_{110}$ crosses the critical value near $\eta_B=1$ and also leads to negative s_1 values when external capture dominates, while $\mathcal{R}_{112}$ and $\mathcal{R}_{121}$ lead to positive s_1 values below $\eta_B=3.3$ and 2.5, respectively, and to negative values beyond.

V. DISCUSSION

Let us now apply these expressions to the $^{16}\mathrm{O}(p,\gamma)^{17}\mathrm{F}$ reaction. The constants defined in Eqs. (22) and (23) take the values $a_N=3.825$ fm and $E_N=1.506$ MeV. Equation (30) provides the approximation

$$S(0)=0.37C_{d5/2}^2+1.58\times 10^{-3}C_{s1/2}^2 \quad \text{keV b}, \tag{36}$$

where $C_{d5/2}$ and $C_{s1/2}$ (expressed in $\mathrm{fm}^{-1/2}$) are the asymptotic normalization constants of the ground state and of the excited state, respectively. The coefficient of the second term is insensitive to the choice of x_0 while the coefficient of the first term is sensitive within a few percents for typical values between $x_0=2$ to 3. The difference between the coefficients in Eq. (36) mostly comes from the binding-energy power $E_B^{2\lambda+1}$ in Eq. (30): the constants N_{E1} do not differ much (4.45 and 3.71, respectively) and the integrals $\mathcal{I}_{11l_f}$ are very close to each other [$\mathcal{I}_{112}(1.584)=1165$ and $\mathcal{I}_{110}(3.783)=1115$, respectively; see Fig. 4]. These values show that the dominance of the transition to the excited state is mainly due to the large value of the asymptotic normalization constant $C_{s1/2}$ with respect to $C_{d5/2}$ (see Table I). This constant is large enough to compensate the effect of the small factor E_B^3. If we slightly vary the exchange parameter of the force, we observe that this constant locally scales as $E_B^{-2.7}$ for the $1/2^+$ state. Hence the large difference between the asymptotic normalization constants is also partly due to the binding energy.

The capture mechanisms to the $5/2^+$ and $1/2^+$ states are qualitatively very similar. Capture to the excited state occurs at larger distances because of a smaller binding energy but this does not affect much $S(0)$. The dominance of $1/2^+$ capture arises from the much larger asymptotic normalization constant of this excited state. If we artificially move the $1/2^+$ state to the same energy as the $5/2^+$ state, the constant $C_{s1/2}$ is reduced to about 8 $\mathrm{fm}^{-1/2}$ but remains significantly larger than for the ground state. This is the only difference which is not due to a smaller binding energy. The interpretation of these results in terms of a halo is then a matter of taste.

The average scattering length plays a negligible role in Eq. (36). Its value is 1.98 fm with the MN force. It introduces relative corrections of order 10^{-4} in the second term and 6×10^{-3} in the smaller first term. A significant effect of the scattering length would require that capture takes place at smaller distances, i.e., would require a larger binding energy. But then the functions $\mathcal{I}_{11l_f}$ would become more sensitive to the choice of x_0 and to other nuclear effects.

The fact that the capture cross sections are larger with the V2 force than with the MN force follows from Eq. (36) and from Table I. This is in agreement with the properties of the ^{17}O mirror nucleus. The asymptotic normalization constants $C_{d5/2}$ of the $^{16}\mathrm{O}+n$ system present a similar behavior [27]. In that case, they are both overestimated with respect to experiment, by about 8% for MN and more than 20% for V2. For ^{17}F, the situation is different for the ground-state constant. The result obtained with MN seems to be too small. Can realistic ^{17}F constants be estimated by scaling the theoretical curves in order to fit the experimental data of Ref. [11]? The fit should be performed at as low energies as possible, but with data with small error bars. We select the data in the energy range 0.4–0.6 MeV. The theoretical S factors obtained with the two forces do not have exactly the same energy dependence from the present energy range to the domain of pure extranuclear capture. Hence scaling them gives different results for the constants. We obtain $C_{d5/2}\approx1.1$ with both forces and $C_{s1/2}\approx78.6$ fm$^{-1/2}$ with V2 and 81.6 fm$^{-1/2}$ with MN. The extrapolation uncertainty due to the force is larger than 3%. These constants introduced in Eq. (36) lead to the estimates

$$S(0)\approx\begin{cases}10.2 & \text{keV b} \quad \text{with V2,}\\ 11.0 & \text{keV b} \quad \text{with MN.}\end{cases} \tag{37}$$

Equation (37) gives an idea of the theoretical uncertainty on the extrapolation, which must be taken into account in addition to experimental uncertainties.

When the binding energy E_B is small, the logarithmic derivative s_1 is the difference of two large numbers since they are both proportional to E_B^{-1}. If these large numbers do not cancel each other, a large value of s_1 is possible. However, this is not a signature of a halo but only of a weak binding.

For the $5/2^+$ ground state, a value around $s_1=0.55$ MeV^{-1} is found with Eq. (34). It is positive because η_B is smaller than the critical value of $\mathcal{R}_{112}$ in Fig. 5. For the $1/2^+$ excited state, one finds $s_1=-5.33$ MeV^{-1}. The lower binding energy of $1/2^+$ allows a much larger $|s_1|$. The value is negative in agreement with the behavior of $\mathcal{R}_{110}$ in Fig. 5.

Let us briefly apply the same expressions to the $^7\mathrm{Be}(p,\gamma)^8\mathrm{B}$ reaction which is also dominated by extranuclear capture. Here $a_N=8.33$ fm and $E_N=0.350$ MeV. The small binding energy $E_B=0.137$ MeV of the 2^+ ground state ($l_i=1$ and $I=1$ or 2) leads to $\eta_B=1.60$, a value similar to the ^{17}F ground-state value. For $E1$ capture from the s wave, Eq. (30) provides for $x_0=2$,

$$S_s(0)=35.8(C_{p12}^2+C_{p22}^2) \quad \text{eV b}, \tag{38}$$

where the coefficient is sensitive to x_0 to less than one percent. Here the asymptotic normalization constants $C_{l_fIJ_f}$ also depend on the channel spin I [12]. The coefficient 35.8 is a little bit smaller than the coefficient 36.5 obtained in Ref. [12] by extrapolating total $S(E)$ values calculated at small energies. The sensitivity to the scattering lengths is very weak. For $E1$ capture from the d wave, one obtains

$$S_d(0)=2.4[C_{p12}^2(1-0.076a_{d1})^2 + C_{p22}^2(1-0.076a_{d2})^2] \quad \text{eV b}, \tag{39}$$

with the notation a_{l_iI} for the average scattering lengths (in fm). This correction is not negligible and might be quite sensitive to the average scattering lengths of the d wave, especially if the a_d are negative as they should be here. With the microscopic model of Ref. [28], we obtain negative scattering lengths but their absolute values are smaller than 0.2 fm. In this case, corrections due to scattering lengths are negligible.

The logarithmic derivative s_1 for an initial s wave is given by Eq. (34) between -2.5 and -2.6 MeV^{-1} depending on the choice for x_0, in agreement with the general behavior of $\mathcal{R}_{101}$ in Fig. 5. For the d wave, $\mathcal{R}_{121}$ is significantly smaller than 3 and one obtains a large positive value near 8.2 MeV^{-1}. The combined $s+d$ value is then -1.9 MeV^{-1} in qualitative agreement with a potential-model study at low energies [29]. However, that study also shows a sensitivity of s_1 to the potential, which would require including a scattering-length dependence in Eq. (35).

VI. CONCLUSIONS

Without any fit, a microscopic description of the $^{16}\mathrm{O}(p,\gamma)^{17}\mathrm{F}$ radiative-capture reaction provides realistic cross sections which are however somewhat overestimated. This overestimation is weaker with the Minnesota force than with the Volkov force V2. These results follow from a corresponding overestimation of the asymptotic normalization constants which could be expected from the properties of the mirror system [27].

At very low energies, the capture process is dominated by large distances. The low-energy asymptotic behavior of all wave functions is well known analytically. We have performed a detailed analysis of zero-energy results. A simple expression is then obtained for the zero-energy S factor, depending only on the asymptotic normalization constants and on an average scattering length of the initial wave. The dependence on this scattering length is negligible in the present case. The expression of $S(0)$ clearly shows that it is here essentially sensitive to the product $E_B^3C_{l_fJ_f}^2$. The asymptotic normalization constant $C_{s1/2}$ of the excited state is large enough to compensate the small factor E_B^3 and to lead to the largest contribution to the capture process at low energies. Its large value is the main difference with ground-state capture and is also related to the lower binding energy of the excited state.

An expression for the logarithmic derivative s_1 of this S factor at zero energy has been derived, which is exact in the context of the extranuclear capture approximation when scattering-length effects are negligible. Under these assumptions, all the properties of s_1 can be explained very simply with functions such as those displayed in Fig. 5. If the value

of these functions calculated with the Sommerfeld parameter of the final bound state is larger than $2\lambda+1$, s_1 is negative and otherwise it is positive. As it is inversely proportional to the binding energy E_B, large $|s_1|$ values may occur for small E_B. These functions can be used to calculate s_1 in other reactions dominated by extranuclear capture, such as $^7\mathrm{Be}(p,\gamma)^8\mathrm{B}$. However, neglecting scattering-length effects is probably not always valid.

We do not think that the differences between the ground-state and excited-state capture properties at low energies are a signature for a halo effect showing up only in the excited state. Indeed, for both states, the capture is essentially extranuclear and we have shown that, to a large extent, differences beween them can be related to the binding energy. Therefore, either both states are considered as halo states because of their weak binding energies, or none of them if the notion of halo is reserved to more remarkable properties requiring at least two loosely bound particles.

ACKNOWLEDGMENTS

This text presents research results of the Belgian program on interuniversity attraction poles initiated by the Belgian-state Federal Services for Scientific, Technical and Cultural Affairs. M.H. is supported by this program. P.D. acknowledges the support of the National Fund for Scientific Research, Belgium.

[1] C.E. Rolfs and W.S. Rodney, *Cauldrons in the Cosmos* (University of Chicago, Chicago, 1988).
[2] Q.K.K. Liu, H. Kanada, and Y.C. Tang, Phys. Rev. C **23**, 645 (1981).
[3] D. Baye and P. Descouvemont, Nucl. Phys. **A407**, 77 (1983).
[4] D. Baye and P. Descouvemont, Ann. Phys. (N.Y.) **165**, 115 (1985).
[5] P. Descouvemont, in *Nuclear Astrophysics*, Proceedings of the International Symposium, Karlsruhe, Germany, 1992, edited by F. Käppeler and K. Wisshak [J. Phys. G Suppl. **19**, S141 (1993)].
[6] K. Langanke, in *Advances in Nuclear Physics*, edited by J.W. Negele and E. Vogt (Plenum, New York, 1994), Vol. 21, p. 85.
[7] D. Baye, in Proceedings of the International Symposium on *Origin and evolution of galaxies*, Atami, Japan, 1997, edited by T. Kajino and S. Kubono (to be published).
[8] K. Wildermuth and Y.C. Tang, in *A Unified Theory of the Nucleus*, edited by K. Wildermuth and P. Kramer (Vieweg, Braunschweig, 1977).
[9] D. Baye and P. Descouvemont, in *Clustering Aspects in Nuclear and Subnuclear Systems*, Kyoto, Japan, 1988, edited by K. Ikeda, K. Katori, and Y. Suzuki [J. Phys. Soc. Jpn. Suppl. **58**, 103 (1989)].
[10] C. Rolfs, Nucl. Phys. **A217**, 29 (1973).
[11] R. Morlock, R. Kunz, A. Mayer, M. Jaeger, A. Müller, J.W. Hammer, P. Mohr, H. Oberhummer, G. Staudt, and V. Kölle, Phys. Rev. Lett. **79**, 3837 (1997).
[12] N.K. Timofeyuk, D. Baye, and P. Descouvemont, Nucl. Phys. **A620**, 29 (1997).
[13] M. Abramowitz and I.A. Stegun, *Handbook of Mathematical Functions* (Dover, New York, 1970).
[14] D. Baye, P.-H. Heenen, M. Libert-Heinemann, Nucl. Phys. **A291**, 230 (1977).
[15] C. Bloch, Nucl. Phys. **4**, 503 (1957).
[16] A.B. Volkov, Nucl. Phys. **74**, 33 (1965).
[17] Y.C. Tang, M. LeMere, and D.R. Thompson, Phys. Rep. **47**, 167 (1978).
[18] D. Baye and N. Pecher, Bull. Cl. Sci., Acad. R. Belg. **67**, 835 (1981).
[19] T. Minamisono, Y. Nojiri, A. Mizugochi, and K. Sugimoto, Nucl. Phys. **A236**, 416 (1974).
[20] P. Swan, Proc. R. Soc. London, Ser. A **228**, 10 (1955).
[21] R.A. Blue and W. Haeberli, Phys. Rev. **137**, B284 (1965).
[22] S. Hara, K.T. Hecht, and Y. Suzuki, Prog. Theor. Phys. **84**, 254 (1990).
[23] S.R. Salisbury, G. Haradie, L. Oppliger, and R. Dangle, Phys. Rev. **126**, 2143 (1962).
[24] M.H. Hull, Jr. and G. Breit, in *Nuclear Reactions II: Theory*, Encyclopedia of Physics, edited by S. Flügge (Springer, Berlin, 1959), Vol. XLI/1, p. 408.
[25] B. Buck, R.A. Baldock, and J.A. Rubio, J. Phys. G **11**, L11 (1985).
[26] R.D. Williams and S.E. Koonin, Phys. Rev. C **23**, 2773 (1981).
[27] D. Baye and N.K. Timofeyuk, Phys. Lett. B **293**, 13 (1992).
[28] P. Descouvemont and D. Baye, Nucl. Phys. **A567**, 341 (1994).
[29] F.C. Barker, Phys. Rev. C **28**, 1407 (1983).